Estimation of Load Side Position in Indirect Drive Robots by Sensor Fusion and Kalman Filtering

Wenjie Chen and Masayoshi Tomizuka

***Abstract*— In indirect drive robot joint, discrepancies exist between the motor side and the load side due to joint flexibilities. Thus, sensor signals may not precisely represent the actual information of interest. In this paper, estimation algorithms for load side information of the indirect robot joint are investigated. Low-cost MEMS sensors, such as gyroscopes and accelerometers, are installed on the load side. Measurement dynamics are incorporated into the model to deal with the sensor noise and bias. Kalman filtering methods are designed based on the extended dynamic/kinematic model using the fusion of multiple sensor signals. Specific issue related to the noise covariance adaptation is studied. The effectiveness of the proposed schemes is experimentally demonstrated and also confirmed in the friction compensation.**

NOMENCLATURE

θ_ℓ	Load side position
$\theta_{\ell,s}$	Sensor measurement of load side position, θ_ℓ
$\dot{\theta}_{\ell,s}$	Sensor measurement of load side velocity, $\dot{\theta}_\ell$
$\ddot{\theta}_{\ell,s}$	Sensor measurement of load side acceleration, $\ddot{\theta}_\ell$
θ_m	Motor side position
$\theta_{m,s}$	Sensor measurement of motor side position, θ_m
b_v	Bias of gyroscope measurement, $\dot{\theta}_{\ell,s}$
b_a	Bias of accelerometer measurement, $\ddot{\theta}_{\ell,s}$
u	Control input, i.e., motor torque
u_s	Sensor measurement of motor torque, u
n_u	Measurement noise of motor torque, u
n_{sm}	Measurement noise of motor side position, θ_m
$n_{v\ell}$	Measurement noise of load side velocity, $\dot{\theta}_\ell$
$n_{a\ell}$	Measurement noise of load side acceleration, $\ddot{\theta}_\ell$
n_{ba}	Fictitious noise of accelerometer bias, b_a
n_{bv}	Fictitious noise of gyroscope bias, b_v
$n_{\ell f}$	Fictitious noise of filtered load side position, $\theta_{\ell f}$
d_j	Joint damping of single-joint system
f_h	Gear meshing friction of single-joint system
f_m	Motor bearing friction of single-joint system
f_ℓ	Load output bearing friction of single-joint system
J_m	Motor side inertia of single-joint system
J_ℓ	Load side inertia of single-joint system
k_j	Joint stiffness of single-joint system
N	Reducer gear ratio of single-joint system

I. INTRODUCTION

In robot applications, discrepancies between the available measurements and the required information set difficulties in achieving good control performance. Such phenomena are resulted from sensor dynamics as well as robot dynamics. Particularly, in robots with joint flexibilities, good motor side performance based on motor side measurements does not guarantee good load side performance, which is a critical issue in practical applications. Precise load side position measurements (e.g., load side encoder), however, are usually not available in industrial robots due to the cost and assembly issues. To overcome this problem, inexpensive MEMS sensors that are easy to mount may be considered. Consideration should be given, however, to problems such as non-negligible biases, limited bandwidth, and noises from low-cost sensors, which set restrictions on the direct utilization of sensor signals. These problems, however, may be circumvented by the proper fusion of multiple sensor signals.

In recent years, estimation algorithms using multi-sensor configurations are studied. Two robust estimation schemes incorporating the Kalman filter and disturbance observer for robot dynamic models have been reported in [1], [2]. These methods require accurate system parameters and thus are not reliable when subjected to model uncertainties. In [3], [4], it has been suggested that a Kalman filtering method based on the kinematic model (KKF) can be formulated by making use of accelerometers and position encoders. The model uncertainties are avoided by using the kinematic relation between the position and the acceleration. These methods, however, were developed mainly for one-mass systems or direct drives (i.e., without indirect drive joint compliance), and the main purpose is velocity estimation while assuming the position information is known. Also, noise covariance in these methods are used as design parameters, which are not easy to select when multiple measurements are utilized.

In this paper, measurement dynamics are introduced into the dynamic/kinematic model to deal with sensor noise and bias. The estimation algorithms (Section II) for indirect drive systems are formulated based on the extended model to fuse the measurements from both the motor side and the load side. Noise covariance adaptation issue is addressed. The schemes are tested by experiments (Section III) and also utilized in the friction compensation (Section IV).

II. ESTIMATION ALGORITHMS

A. Model for Measurement Dynamics

The bias and the noise in the sensor output can be described as

$$\dot{b}(t) = n_b(t) \tag{1a}$$

$$x_s(t) = x(t) + b(t) + n_s(t) \tag{1b}$$

This work was supported by FANUC Ltd., Japan. Real-time control hardware and software were provided by National Instruments, Inc.

Wenjie Chen and Masayoshi Tomizuka are with the Department of Mechanical Engineering, University of California at Berkeley, Berkeley, CA 94720, USA. Email: {wjchen, tomizuka}@me.berkeley.edu

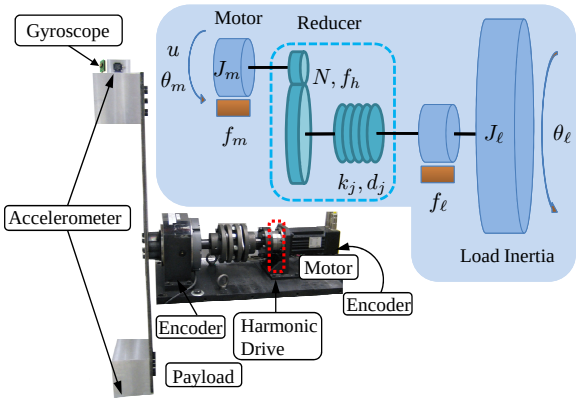

Fig. 1. Single-Joint Indirect Drive System Setup

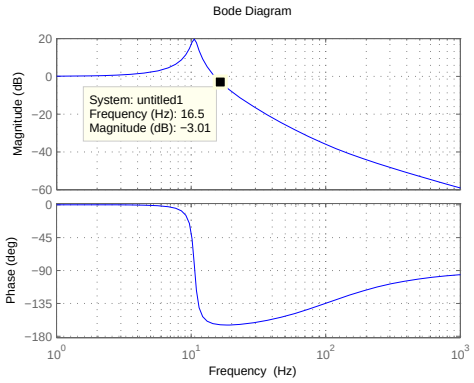

Fig. 2. Bode Plot of $\frac{\theta_\ell(s)}{\lambda_0\theta_m(s)}$ for the System in Fig. 1

where b is the bias of the sensor output, and n_b is a fictitious noise. x is the actual physical quantity to be measured, x_s is the sensor output, and n_s is the measurement noise.

B. System Dynamic Model

Suppose that the state-space model of an indirect robot joint is

$$\dot{x} = Ax + Bu. \tag{2}$$

A typical indirect drive system shown in Fig. 1 is modeled as a two-mass system where $x = \begin{bmatrix}\theta_m & \dot{\theta}_m & \theta_\ell & \dot{\theta}_\ell\end{bmatrix}^{\mathrm{T}}$, A is the 4×4 system matrix, and B is the 4×1 input vector. The setup in Fig. 1 will be used in Section III for experimental study.

If the load side is equipped with both the gyroscope and the accelerometer, the system model (2) with measurement dynamics is extended to

$$\dot{x}_m(t) = \mathcal{A}_m x_m(t) + \mathcal{B}_{m,u}u_s(t) + \mathcal{B}_{m,w}w_m(t) \tag{3a}$$
$$y_m(t) = \mathcal{C}_m x_m(t) + v_m(t) \tag{3b}$$

where for the system in Fig. 1

$$x_m = \begin{bmatrix}x^{\mathrm{T}} & b_a & b_v\end{bmatrix}^{\mathrm{T}} \in \mathbb{R}^{6\times 1}$$
$$y_m = \begin{bmatrix}\theta_{m,s} & \dot{\theta}_{\ell,s} & \ddot{\theta}_{\ell,s}\end{bmatrix}^{\mathrm{T}} \in \mathbb{R}^{3\times 1}$$
$$w_m = \begin{bmatrix}n_u & n_{ba} & n_{bv}\end{bmatrix}^{\mathrm{T}} \in \mathbb{R}^{3\times 1}$$
$$v_m = \begin{bmatrix}n_{sm} & n_{v\ell} & n_{a\ell}\end{bmatrix}^{\mathrm{T}} \in \mathbb{R}^{3\times 1}$$
$$\mathcal{A}_m = \left[\begin{array}{c|c} A & \mathbf{0} \\ \hline \mathbf{0} & \mathbf{0}\end{array}\right] \in \mathbb{R}^{6\times 6}$$
$$\mathcal{B}_{m,u} = \left[\begin{array}{c|c} B & \mathbf{0}\end{array}\right]^{\mathrm{T}} \in \mathbb{R}^{6\times 1}$$
$$\mathcal{B}_{m,w} = \left[\begin{array}{c|c} B & \mathbf{0} \\ \hline \mathbf{0} & I_2\end{array}\right] \in \mathbb{R}^{6\times 3}$$
$$\mathcal{C}_m = \left[\begin{array}{cccc|cc} 1 & 0 & 0 & 0 & 0 & 0 \\ 0 & 0 & 0 & 1 & 0 & 1 \\ \hline \multicolumn{4}{c|}{A_4} & 1 & 0\end{array}\right] \in \mathbb{R}^{3\times 6}$$

A_4 is the fourth row of the matrix A, and I_n is the $n\times n$ identity matrix.

Based on the above extended system dynamic model, a Kalman filter can be formulated to estimate the load side information, which is described in Section II-D.

C. System Kinematic Model

The kinematic model from the acceleration to the position on the load side can be written as

$$\frac{d}{dt}\begin{bmatrix}\theta_\ell(t) \\ \dot{\theta}_\ell(t)\end{bmatrix} = \begin{bmatrix}0 & 1 \\ 0 & 0\end{bmatrix}\begin{bmatrix}\theta_\ell(t) \\ \dot{\theta}_\ell(t)\end{bmatrix} + \begin{bmatrix}0 \\ 1\end{bmatrix}\ddot{\theta}_\ell(t) \tag{4}$$

The Kalman filter based on the kinematic model (4) is called the kinematic Kalman filter (KKF) [3]. In KKF, the acceleration is used as an input to the filter, and the position information is used to correct the estimation output. In the indirect robot joint, however, precise load side position measurement (e.g., load side encoder) is usually not available, which makes it difficult to directly utilize the KKF algorithm.

Let $G_{m2l}(s)$ be the transfer function from the motor side position θ_m to the load side position θ_ℓ, i.e., $G_{m2l}(s) \triangleq \frac{\theta_\ell(s)}{\theta_m(s)}$. By the inherent system dynamics ((14) in Section III-A), $G_{m2l}(s)$ is approximately zero-phase static gain at the low frequency region (Fig. 2), since the dynamic chain from θ_m to θ_ℓ can be modeled by mass, gear, spring and damper. This indicates that the low frequency component of θ_ℓ can be approximated by that of θ_m.

Pass θ_m and θ_ℓ through a first order low pass filter $G_f(s) = \frac{\alpha}{s+\alpha}$, where $\alpha = \beta f_b$, f_b is the bandwidth of $G_{m2l}(s)$, and $\beta \in (0,\infty)$ is a design parameter for the low pass filter. Let the filter outputs be θ_{mf} and $\theta_{\ell f}$, respectively. It follows that

$$\dot{\theta}_{mf} = -\alpha\theta_{mf} + \alpha\theta_m \tag{5a}$$
$$\dot{\theta}_{\ell f} = -\alpha\theta_{\ell f} + \alpha\theta_\ell \tag{5b}$$

The above analysis shows that, if β is chosen properly, the filter outputs will have the following relation

$$\theta_{\ell f} \approx \lambda_0\theta_{mf} \tag{6}$$

where λ_0 is the DC gain of $G_{m2l}(s)$ (e.g., $\lambda_0 = \frac{1}{N}$ for the system in Fig. 1). Generally, it is desired that $\beta \le 1$ and thus $\alpha \le f_b$.

The filter dynamics (5) and the measurement dynamics (1) can be added into the system kinematic model (4), giving

$$\dot{x}_k(t) = \mathcal{A}_k x_k(t) + \mathcal{B}_{k,u}\ddot{\theta}_{\ell,s}(t) + \mathcal{B}_{k,w}w_k(t) \tag{7a}$$
$$y_k(t) = \mathcal{C}_k x_k(t) + v_k(t) \tag{7b}$$

where for the system in Fig. 1

$$
\begin{aligned}
x_k &= \begin{bmatrix} \theta_{\ell f} & \theta_\ell & \dot{\theta}_\ell & b_a & b_v \end{bmatrix}^{\mathrm{T}} \in \mathbb{R}^{5\times 1} \\
y_k &= \begin{bmatrix} \theta_{\ell f,s} & \dot{\theta}_{\ell,s} \end{bmatrix}^{\mathrm{T}} \in \mathbb{R}^{2\times 1} \\
w_k &= \begin{bmatrix} n_{a\ell} & n_{ba} & n_{bv} \end{bmatrix}^{\mathrm{T}} \in \mathbb{R}^{3\times 1} \\
v_k &= \begin{bmatrix} n_{\ell f} & n_{v\ell} \end{bmatrix}^{\mathrm{T}} \in \mathbb{R}^{2\times 1} \\
\mathcal{A}_k &= \left[\begin{array}{cccc|c} -\alpha & \alpha & 0 & 0 & \\ 0 & 0 & 1 & 0 & \mathbf{0} \\ 0 & 0 & 0 & 1 & \\ \hline \multicolumn{4}{c|}{\mathbf{0}} & \mathbf{0} \end{array}\right] \in \mathbb{R}^{5\times 5} \\
\mathcal{B}_{k,u} &= \begin{bmatrix} 0 & 0 & 1 & 0 & 0 \end{bmatrix}^{\mathrm{T}} \in \mathbb{R}^{5\times 1} \\
\mathcal{B}_{k,w} &= \left[\begin{array}{c|c} \mathbf{0} & I_3 \end{array}\right]^{\mathrm{T}} \in \mathbb{R}^{5\times 3} \\
\mathcal{C}_k &= \begin{bmatrix} 1 & 0 & 0 & 0 & 0 \\ 0 & 0 & 1 & 0 & 1 \end{bmatrix} \in \mathbb{R}^{2\times 5}
\end{aligned}
$$

By the approximation in (6), $\lambda_0\theta_{mf,s}$, where $\theta_{mf,s}(s) = G_f(s)\theta_{m,s}(s)$, can be used as the fictitious measurement for the model output $\theta_{\ell f,s}$, and the noise covariance of $\theta_{\ell f,s}$ can be approximated by the noise covariance of $\lambda_0\theta_{mf,s}$, or could be designed for the following Kalman filter.

D. Kalman Filtering

The discrete time form of the extended system model (3) or (7) can be described as

$$x_d(k+1) = \mathcal{A}_d x_d(k) + \mathcal{B}_{d,u} u_d(k) + \mathcal{B}_{d,w} w_d(k) \tag{8a}$$

$$y_d(k) = \mathcal{C}_d x_d(k) + v_d(k) \tag{8b}$$

where $x_d(k)$, $y_d(k)$, $u_d(k)$, $w_d(k)$, and $v_d(k)$ are the k-th time step sampled values of $x_m(t)$, $y_m(t)$, $u_s(t)$, $w_m(t)$, and $v_m(t)$ for the system dynamic model (3), and $x_k(t)$, $y_k(k)$, $\ddot{\theta}_{\ell,s}(t)$, $w_k(t)$, and $v_k(t)$ for the system kinematic model (7), respectively. $\mathcal{A}_d$, $\mathcal{B}_{d,u}$, $\mathcal{B}_{d,w}$, and $\mathcal{C}_d$ are derived from (3) or (7) by the zero-order-hold (ZOH) method. In practice, $\mathcal{B}_{d,w}w_d$ could be generalized to include the disturbance and/or mismatched model dynamics.

For the extended system model (8), a Kalman filter to estimate the system states is given by

$$\hat{x}_d(k) = \hat{x}_d^o(k) + L_d(k)\tilde{y}_d^o(k) \tag{9a}$$

$$\hat{x}_d^o(k+1) = \mathcal{A}_d\hat{x}_d(k) + \mathcal{B}_{d,u}u_d(k) \tag{9b}$$

$$\tilde{y}_d^o(k) = y_d(k) - \mathcal{C}_d\hat{x}_d^o(k) \tag{9c}$$

where the Kalman filter gain L_d is calculated as

$$L_d(k) = M_d(k)\mathcal{C}_d^{\mathrm{T}}[\mathcal{C}_d M_d(k)\mathcal{C}_d^{\mathrm{T}} + \hat{V}_d(k)]^{-1} \tag{10a}$$

$$M_d(k+1) = \mathcal{A}_d Z_d(k)\mathcal{A}_d^{\mathrm{T}} + \mathcal{B}_{d,w}\hat{W}_d(k)\mathcal{B}_{d,w}^{\mathrm{T}} \tag{10b}$$

$$Z_d(k) = M_d(k) - L_d(k)\mathcal{C}_d M_d(k) \tag{10c}$$

where $\hat{W}_d(k)$ and $\hat{V}_d(k)$ are the covariance estimates of $w_d(k)$ and $v_d(k)$, respectively. $M_d(k)$ and $Z_d(k)$ are the one-step a-priori and a-posteriori covariances of the state estimation error, respectively. Note that $(\mathcal{A}_d, \mathcal{C}_d)$ is observable and $(\mathcal{A}_d, \mathcal{B}_{d,w})$ is controllable. Thus, if $w_d(k)$ and $v_d(k)$ are stationary zero-mean Gaussian white noises, the Kalman filter gain L_d, the covariance matrices M_d and Z_d will converge to stationary matrices. However, $w_d(k)$ and $v_d(k)$ are often interpreted as fictitious noise terms and their covariances are adjusted to assign a reasonable set of closed loop eigenvalues to the estimator [4]. Another way to deal with these covariances is to use the adaptive scheme in the next section.

The proposed method can also be formulated in a similar way without the gyroscope measurement in the model output in (3) or (7). However, it is better to include the gyroscope measurement, since $\theta_{lf,s}$ uses a fictitious measurement $\lambda_0\theta_{mf,s}$ to formulate KKF, and $\dot{\theta}_{\ell,s}$ is the only real load side measurement in the KKF model output in (7).

The KKF has several advantages compared with the dynamic model based Kalman filter (DKF) [4]. Firstly, system representation using kinematic model is simpler than the one using dynamic model. Secondly, the kinematic model is an exact representation of the system states. It involves neither physical parameters nor external disturbances. Thus no model uncertainties need to be considered in KKF.

E. Estimation of Noise Covariance

As an optimal stochastic estimator, the Kalman filter assumes linear model and Gaussian additive noises with known covariances. In reality, however, it is difficult to get the accurate covariances of the process or measurement noises. Thus, particular interest has been focused on the estimation of the noise covariances, i.e., $\hat{W}_d(k)$ and $\hat{V}_d(k)$.

In the proposed Kalman filter, the bias noises (n_{ba} and n_{bv}), and the output $\theta_{lf,s}$, are fictitious and their covariances cannot be physically identified. Practically, if the measurement bias is time invariant or slowly varying, it is desired that the fictitious bias covariance should be large enough at the beginning to steer the bias estimate quickly to its actual value. Then the fictitious noise covariance should be decreased to reduce the sensitivity of the bias estimation.

To handle uncertainties in these covariances, an adaptive approach utilizing the residual information to estimate the noise covariances is applied. The routines presented here are modified from the algorithms summarized in [5], [6], which were developed based on the principle of maximum likelihood estimate.

By comparing the a-priori and a-posteriori state estimates, the process noise covariance estimate $\hat{W}_d(k)$ is updated by

$$\begin{aligned}\hat{W}_d^*(k) = \mathcal{B}_{d,w}^{-1}[&\Delta x_d(k)\Delta x_d^{\mathrm{T}}(k) + Z_d(k) \\ &- \mathcal{A}_d Z_d(k-1)\mathcal{A}_d^{\mathrm{T}}](\mathcal{B}_{d,w}^{-1})^{\mathrm{T}}\end{aligned} \tag{11a}$$

$$\Delta x_d(k) = \hat{x}_d(k) - \hat{x}_d^o(k) \tag{11b}$$

$$\hat{W}_d(k+1) = \hat{W}_d(k) + [\hat{W}_d^*(k) - \hat{W}_d(k)]/N_w \tag{11c}$$

where the adaptive estimate $\hat{W}_d^*(k)$ is shown to be the residual pseudo-covariance plus the change of the a-posteriori covariance between the two consecutive time steps. The current step covariance estimate $\hat{W}_d(k)$ is then updated to this estimate $\hat{W}_d^*(k)$ in a moving average manner with N_w as the window size. Note that, if $\mathcal{B}_{d,w}$ is not invertible, $\mathcal{B}_{d,w}^{-1}$ in (11a) can be replaced by the following pseudo-inverse

$$\mathcal{B}_{d,w}^{\#} = \left(\mathcal{B}_{d,w}^{\mathrm{T}}\mathcal{B}_{d,w}\right)^{-1}\mathcal{B}_{d,w}^{\mathrm{T}} \tag{12}$$

Similarly, the measurement noise covariance estimate, $\hat{V}_d(k)$, can be adaptively updated by

$$\hat{V}_d^*(k) = \Delta y_d(k)\Delta y_d^{\mathrm{T}}(k) + \mathcal{C}_d Z_d(k)\mathcal{C}_d^{\mathrm{T}} \quad (13a)$$

$$\Delta y_d(k) = y_d(k) - \mathcal{C}_d \hat{x}_d(k) \quad (13b)$$

$$\hat{V}_d(k+1) = \hat{V}_d(k) + [\hat{V}_d^*(k) - \hat{V}_d(k)]/N_v \quad (13c)$$

where $\Delta y_d(k)$ is not the innovation but the a-posteriori estimation error. The physical interpretation of this solution is that the theoretical value of measurement noise covariance should match with the estimation residual covariance.

Note that, the above adaptation for the process (or measurement) noise covariance estimate, $\hat{W}_d$ (or $\hat{V}_d$), is the approximate solution developed separately assuming the actual covariance V_d (or W_d) is known [6]. The two solutions can be used, with caution, to estimate both covariances simultaneously, or can be implemented one after another in the serial way, or can be confined to adapt $\hat{W}_d$ (or $\hat{V}_d$) only. Also, the adaptive performance is sensitive to the window sizes of the moving average filters. Thus, they should be carefully selected for each application.

III. EXPERIMENTAL STUDY

A. Experimental Setup

The proposed methods were implemented on a single-joint indirect robot shown in Fig. 1. This experimental setup consists of: 1) a servo motor with a $20,000$ counts/revolution encoder, 2) a harmonic drive with a 80:1 gear ratio, 3) a load-side $144,000$ counts/revolution encoder, 4) and a payload. The anti-resonant and resonant frequencies of the setup are approximately 11Hz and 19Hz, respectively.

The load side encoder is used only for performance evaluation. Besides the encoder, two other kinds of sensors are available on the load side. A MEMS gyroscope (Analog, Type: ADXRS150) is installed at one end of the payload. Two accelerometers (Kistler, Type: 8330A3) are installed at the two ends of the payload symmetrically as shown in Fig. 1 to compensate for the gravity effects on the measurements.

Finally, the algorithms were implemented in a LabVIEW real-time target installed with LabVIEW Real-Time and FPGA modules. The sampling rate was selected to be 1kHz.

The system dynamic model can be written as

$$J_m\ddot{\theta}_m = -\frac{1}{N}\left[k_j\left(\frac{\theta_m}{N} - \theta_\ell\right) + d_j\left(\frac{\dot{\theta}_m}{N} - \dot{\theta}_\ell\right)\right] + u - (f_m + f_h) \quad (14a)$$

$$J_\ell\ddot{\theta}_\ell = k_j\left(\frac{\theta_m}{N} - \theta_\ell\right) + d_j\left(\frac{\dot{\theta}_m}{N} - \dot{\theta}_\ell\right) - f_\ell \quad (14b)$$

The state-space formulation of this dynamic model can be derived by ignoring the nonlinear friction terms.

B. Load Side Estimation Experiments

The above DKF and KKF methods were compared with the one using only motor encoder output $\theta_{m,s}$, in which case the load side position estimation error is given by the joint torsion $\delta_{\ell,s} = \frac{\theta_{m,s}}{N} - \theta_{\ell,s}$.

TABLE I

THE PARAMETER VALUES USED IN THE EXPERIMENTS (SI UNITS)

$\mathrm{cov}(n_u)$	$\mathrm{cov}(n_{sm})$	$\mathrm{cov}(n_{\ell f,s})$	$\mathrm{cov}(n_{v\ell})$
10^{-4}	8.225×10^{-9}	8.225×10^{-9}	2.525×10^{-5}
$\mathrm{cov}(n_{a\ell})$	$\mathrm{cov}(n_{bv})$	$\mathrm{cov}(n_{ba})$	β
3.284×10^{-3}	10^{-4}	0.1	0.5
J_m	J_ℓ	k_j	d_j
5.313×10^{-4}	8.16	2.4×10^4	47

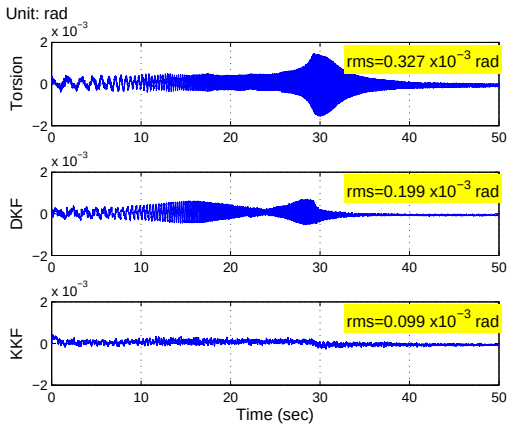

Fig. 3. Estimation Errors of Load Side Position in Chirp Experiment

The first experiment was to test the effectiveness of the proposed algorithms in the open loop frequency rich response. The motor torque command was a quadratic chirp signal with the magnitude of 0.2Nm. The frequency range varied from 0.5Hz to 50Hz quadratically in 50sec.

The initial noise covariances and the dynamic model parameters used in the algorithms are listed in Table I. These are mostly the nominal values identified experimentally, except for the covariance of n_u, $n_{\ell f,s}$, n_{ba}, and n_{bv}. Also, J_l and k_j were added with 20% error to check the performance of DKF when subjected to the parameter uncertainty. Note that β in the KKF method was selected as 0.5, i.e., $\alpha = 0.5 f_b$. The adaptive covariance estimation scheme was confined to adapt $\hat{V}_d$ only.

In Fig. 3, the rms value on the right top of each sub-figure denotes the root mean square value of the load side position estimation error. It shows that the KKF method achieves the best estimation performance, where the estimation error is greatly reduced upon all the testing frequency range. The DKF method does not perform as good as KKF, and it amplifies the estimation error at some frequency range due to the parameter uncertainty.

The adapted $\hat{V}_d$ in both methods is shown in Fig. 4. As expected, to match the covariance with the estimation results, $\hat{V}_d$ is tended to increase when the estimation error is increasing (especially around the resonant frequency 19Hz).

Fig. 5 shows that both methods are effective to estimate the biases of gyroscope and accelerometer outputs. Thus, the bias effects in the utilization of sensor signals are attenuated.

Another experiment was to verify the effectiveness of the methods for specific tracking trajectory. The desired load side

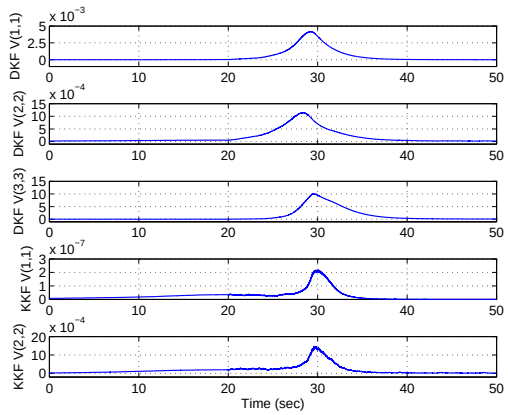

Fig. 4. Covariance Estimation in Chirp Experiment

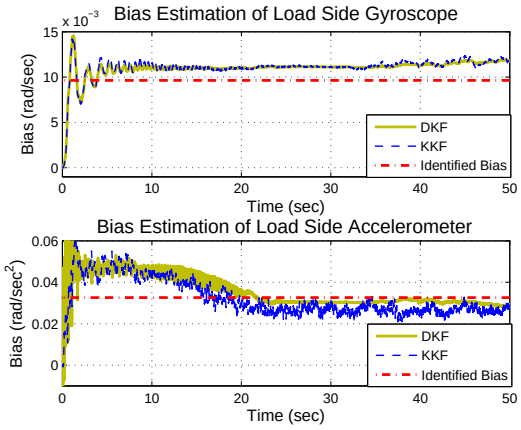

Fig. 5. Bias Estimation in Chirp Experiment

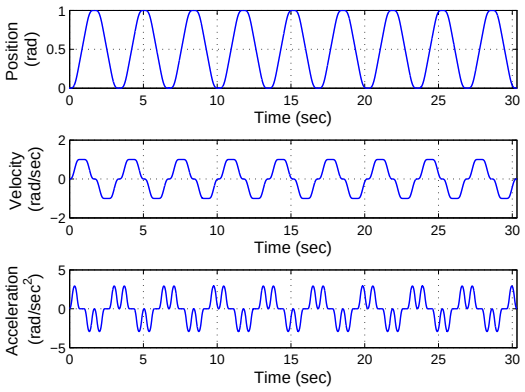

Fig. 6. Load Side Desired Trajectory

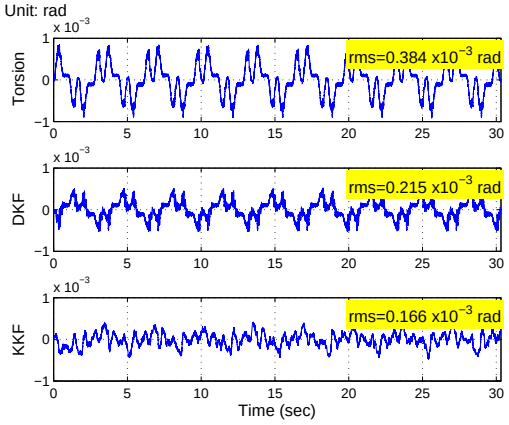

Fig. 7. Estimation Errors of Load Side Position in Trajectory Experiment

trajectory is shown in Fig. 6, which was designed based on the fourth-order trajectory suggested in [7]. The feedback controller used here is illustrated in Fig. 9 without any friction compensation, i.e., $\hat{F} = \hat{f}_\ell = 0$ in (15)-(16). All the covariances and parameter values remained the same as in the chirp experiment (Table I) except for the window size N_v used in the covariance adaptation scheme.

The result of this experiment is shown in Fig. 7, where KKF still achieves the best estimation performance. It is seen that the estimation error by KKF is oscillatory. It is mainly due to the transmission error effect [8], since this effect is not considered in the estimation algorithm. Fig. 8 illustrates the actual and estimated tracking error of the load side position in this experiment. It shows that the tracking error estimated by KKF captures most trends of the actual tracking error. Therefore, the KKF method could be utilized in the load side position tracking application, e.g., friction compensation.

IV. APPLICATION: FRICTION COMPENSATION

In indirect drive systems, friction, one of the main factors that diminish control performance, affects the controlled plant on the load side as well as the motor side. In [9], a friction compensation scheme for indirect drive trains was developed in the absence of precise load side measurements. The scheme in [9] compensates for the friction effects on both the motor side and the load side. Here, however, only the load side compensation which utilizes the estimated position is introduced to demonstrate the effectiveness of the estimation algorithm.

A. Controller Structure

Fig. 9 shows the overall control structure of the single-joint indirect drive system. The feedforward controller, F_2, is designed as

$$u_{ff}(t) = J_m \ddot{\theta}_{md}(t) + \frac{1}{N} J_\ell \ddot{\theta}_{\ell d}(t) + \hat{F}(t) \qquad (15)$$

where $\hat{F}$ is the estimated entire friction force. $\ddot{\theta}_{\ell d}$ is the desired load side acceleration. θ_{md} is the motor side position reference generated by F_1 from the desired load side position, $\theta_{\ell d}$, i.e.

$$\theta_{md}(t) = \frac{N}{k_j}\left[J_\ell \ddot{\theta}_{\ell d}(t) + \hat{f}_\ell(t)\right] + N\theta_{\ell d}(t) \qquad (16)$$

where $\hat{f}_\ell$ is the estimated load side friction.

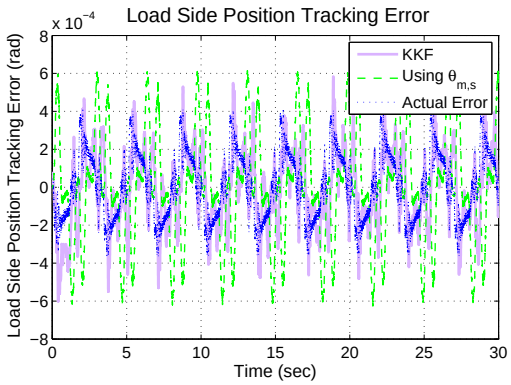

Fig. 8. Load Side Actual and Estimated Position Tracking Error

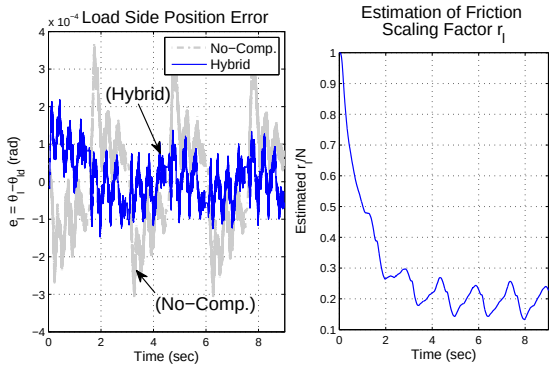

Fig. 10. Performance of the Hybrid Friction Compensator

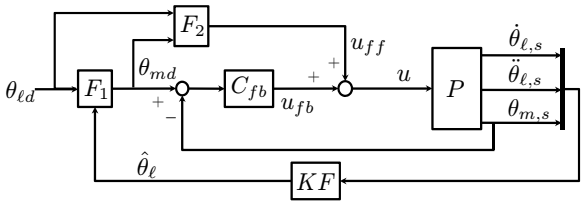

Fig. 9. Block Diagram of the Overall Control System

The feedback controller, C_{fb}, is selected as

$$C_{fb}(s) = \left(k_v + \frac{k_i}{s}\right)(s + k_p) \tag{17}$$

where k_p is the gain of the position loop, k_v and k_i are the gains of the velocity loop. The above controller is discretized by the Euler method for implementation.

An adaptive friction observer is designed to obtain $\hat{F}$, i.e.

$$\hat{F} = \hat{K}^{\mathrm{T}}\hat{\Phi} \tag{18}$$

where $\hat{K}$ and $\hat{\Phi}$ are defined and adapted as in [9].

In [9], the load side friction, f_ℓ, is modeled as a scaled quantity of the entire friction force, F. Thus, once $\hat{F}$ is adapted successfully on the motor side, f_ℓ can be estimated as

$$\hat{f}_\ell = \hat{r}_\ell \hat{F} \tag{19}$$

where $\hat{r}_\ell$ is the estimated scaling factor obtained by

$$\dot{\hat{r}}_\ell = -\gamma_{r_\ell}\hat{F}\hat{e}_\ell, \quad \hat{e}_\ell = \hat{\theta}_\ell - \theta_{\ell d} \tag{20}$$

where $\gamma_{r_\ell} > 0$ is the adaptation gain, and $\hat{\theta}_\ell$ is the estimated load side position produced by some estimation algorithm.

B. Load Side Friction Compensation Experiment

In Fig. 8, the offset in the tracking error, which is partly due to the load side friction effects, can be successfully estimated by the KKF method. Therefore, KKF is employed in (20) to obtain the load side position estimate, $\hat{\theta}_\ell$.

To show the effectiveness of the load side compensation algorithm, $\hat{r}_\ell$ was initialized to $1.0N$ (the reducer gear ratio). Fig. 10 illustrates the performance of friction compensator enabled on both the motor side and the load side (Hybrid), compared to the case without any friction compensation (No-Comp.). It is seen that the load side position tracking error offset is significantly reduced by the compensator scheme, while the remaining tracking error is mainly due to the transmission error effect [8], [9]. It also shows that the compensator performance converges to a sub-optimal stage in less than 1 repeated trajectory.

V. CONCLUSIONS

This paper presented the estimation algorithms for load side information of indirect robot joint based on a multi-sensor configuration. Kalman filtering methods were formulated on the extended dynamic/kinematic model taking measurement dynamics (bias and noise) into consideration. Noise covariance adaptation was studied. The effectiveness of the methods was verified experimentally on a single-joint indirect robot. The KKF method was also successfully applied to the friction compensation application.

REFERENCES

[1] K. Heui-Wook and S. Seung-Ki, "A new motor speed estimator using kalman filter in low-speed range," *Industrial Electronics, IEEE Transactions on*, vol. 43, no. 4, pp. 498–504, 1996.

[2] K. SangJoo, C. Wan Kyun, and Y. Youngil, "A combined observer for robust state estimation and kalman filtering," in *Proceedings of the 2003 American Control Conference*, vol. 3, 2003, pp. 2459–2464.

[3] D. J. Lee and M. Tomizuka., "State/parameter/disturbance estimation with an accelerometer in precision motion control of a linear motor," in *ASME Internation Mechatronics Engineering Congress and Exposition*, 2001.

[4] S. Jeon and M. Tomizuka, "Benefits of acceleration measurement in velocity estimation and motion control," *Control Engineering Practice*, vol. 15, no. 3, pp. 325–332, 2007.

[5] R. Mehra, "Approaches to adaptive filtering," *Automatic Control, IEEE Transactions on*, vol. 17, no. 5, pp. 693–698, 1972.

[6] P. S. Maybeck, *Stochastic Models, Estimation, and Control*. New York: Academic Press, Inc., 1982, vol. 2.

[7] P. Lambrechts, M. Boerlage, and M. Steinbuch, "Trajectory planning and feedforward design for electromechanical motion systems," *Control Engineering Practice*, vol. 13, no. 2, pp. 145–157, 2005.

[8] C.-H. Han, C.-C. Wang, and M. Tomizuka, "Suppression of vibration due to transmission error of harmonic drives using peak filter with acceleration feedback," in *Proceedings of the 10th IEEE International Workshop on Advanced Motion Control*, 2008, pp. 182–187.

[9] W. Chen, K. Kong, and M. Tomizuka, "Hybrid adaptive friction compensation of indirect drive trains," in *Proceedings of 2009 ASME Dynamic Systems and Control Conference*, Oct. 2009.